Modularisation of published and novel models toward a complex KIR2DL4 pathway in pbNK cell

Nurul Izza Ismail (nurul.ismail@usm.my)
Universiti Sains Malaysia

Research Article

Keywords: model, pathway, kir2dl4, models, receptor, natural

Posted Date: August 19th, 2021

DOI: https://doi.org/10.21203/rs.3.rs-593814/v1

RESEARCH

Modularisation of published and novel models toward a complex KIR2DL4 pathway in pbNK cell

Nurul Izza Ismail*

Correspondence: nurul.ismail@usm.my
School of Biological Sciences, Universiti Sains Malaysia, 11800USM Penang, Malaysia
Full list of author information is available at the end of the article

*Equal contributor

Abstract

KIR2DL4 is an interesting receptor expressed on the peripheral blood natural killer (pbNK) cell as it can be either activating or inhibitory depending on the amino acid residues in the domain. This model uses mathematical modelling to investigate the downstream effects of natural killer cells' activation (KIR2DL4) receptor after stimulation by key ligand (HLA-G) on pbNK cells. Development of this large pathway is based on a comprehensive qualitative description of pbNKs' intracellular signalling pathways leading to chemokine and cytotoxin secretion, obtained from the KEGG database (https://www.genome.jp/kegg-bin/show pathway?hsa04650). From this qualitative description we built a quantitative model for the pathway, reusing existing curated models where possible and implementing new models as needed. This large pathway consists of two published sub-models; the Ca^{2+} model and the NFAT model, and a newly built FCεRIγ sub-model. The full pathway was fitted to HLA-G-KIR2DL4 pathway published dataset and the model that we developed fitted well to one of two secreted cytokines. The model can be used topredict the production of IFNγ and TNFα cytokines.

Keywords: HLA-G; KIR2DL4; mathematical model; modulation; signalling pathway

Background

Natural killer (NK) cells being primarily associated with innate immunity. There is some evidence that they also contribute to adaptive immunity, especially in adapting the environment through priming, education and memory, and are able to respondto multiple infections from a particular antigen [1, 2, 3]. They comprise approximately 15% of all circulating lymphocytes [4, 5, 6] including 2-18% of lymphocytes in human peripheral blood. NK cells have the capability to lyse or destroy some abnormal cells - for example, tumour cells and virus-infected cells and are known as effector cells,

which means they selectively bind to ligands and regulate target cells' biological activities [7, 8]. NK cell function is determined by a balance of activation and inhibition signalling induced by trans-membrane receptors [9, 1]. This process involves engagement of ligands with the receptors, as well as the actionof pro-inflammatory cytokines such as IL-1, IL-2, IL-12, IL-15, IL-18, IL-21 and IFNα, β [7, 10, 11]. If activation signalling dominates, NK cells become activated. Upon contact with other cells recognised as undesirable, activated NK cells are able to mediate cell killing via two mechanisms, exocytosis of perforin/granzyme granules and signalling via TNF receptors [12].

The interaction between NK cells and target cells requires docking between NK cell receptors and target cell ligands. In this study, we developed a model to predict the production of IFNγ and TNFα cytokines induced by the binding of HLA-Gto endocytosed KIR2DL4 receptor as shown in Figure 1. The KIR2DL4 receptoris an endocytosed receptor. The transient passage of endocytosed KIR2DL4 receptor at the cell surface occurs when an NK cell is activated by IL-2. The transient passage of KIR2DL4 at the cell surface is sufficient to capture soluble HLA-G andtransport it to the endosomes. The endocytosed HLA-G/KIR2DL4 complex recruits FCεRIγ and aggregates the FC. Activation of FCεRIγ by Lyn-catalysed phosphorylation then recruits Syk. Syk binding to FCεRIγ is activated via phosphorylation by Lyn. Phosphorylated Syk then phosphorylates GRB2-associated binding protein 2 (GAB2), which leads to activation of the phosphoinositide 3-kinase (PI3K) signalling cascade. One pathway activated by HLA-G through PI3K is the PLCγ- IP3-Ca-CaN-NFAT cascade. Ligation of FCεRIγ stimulates expression of many cytokines via a Ca-dependent mechanism. The PLCγ-IP3-Ca-CaN-NFAT cascade also can be activated by active Syk/ZAP70 via LAT. PI3K and LAT activate phospholipase C gamma (PLCγ). The role of PLCγ is to control the concentration of calciumin the cell [13, 14] through IP3. PLCγ catalyses the conversion of IP3 from PIP2. IP3 causes the release of Ca^{2+} from the intracellular endoplasmic reticulum. Ca^{2+} binds to calcineurin (CaN), and the complex then dephosphorylates the nuclear factor in an activated T-cell (NFAT). The migration of NFAT into the cell nucleus starts the transcription of cytokines TNFα and IFNγ [15, 16].

The signalling pathway to be modelled, depicted in Figure 2 consist of many components and reactions. We apply modular design principles into the construction of NK signalling model. This model incorporates two published models including the Ca^{2+} oscillations of Dupont and Erneux (1997) [17] and NFAT cycling of Cooling et al. (2009) [18]. A new sub-model was built to complete the signalling pathway, based on the availability of experimental data. One sub-model was developed in this section and termed FCεRIγ and appear as Level 2 models in Figure 2. With all required sub-models developed, we were then able to bring together these modelsinto a complete HLA-G-KIRDL4 pathway and labelled as Level 3 in Figure 2.

Results

Re-using and implementing models from Physiome Model Repository (level 1 models)

Ca^{2+} oscillations in Dupont and Erneux, 1997

This section outlines the model labelled as Ca^{2+} sub-model in Figure 2. Dupont and Erneux simulated a model that captures the oscillation of Ca^{2+} in a cell in responseto upstream signalling (Figure 3) [17]. The repository associated with thismodel can be found at https://github.com/Nurulizza/HLAG_to_cytokine/tree/master/dupont_1997.

Our pathway does not include the production of IP4 by phosphorylated IP3. To exclude this reaction, we zeroed the V_{3k} reaction in Dupont's model which representsthe activity of IP3 3-kinase in catalysing the IP4 production. In this case, when the maximal velocity of 3-kinase is zero, and the activity of 5-phosphatase very much exceeds the activity of 3-kinase, oscillations in IP3 disappear. The behaviour has also been observed in studies of other cell types [19, 20, 21]. The Ca^{2+} and IP3 behaviour in the system without the activity of 3-kinase is illustrated in Figure 4. Asexpected, we retained the oscillation of Ca^{2+} and the oscillation of IP3 disappeared without the changes of IP3 into IP4.

NFAT cycling in Cooling et al., 2009

This section describes the model labelled as NFAT sub-model in Figure 2. Coolinget al. [18] adapted the experimental protocol of Tomida et al. [22], as described in previously to model NFAT cycling (Figure 5). The respository associated with this model can be found at https://github.com/Nurulizza/HLAG_to_cytokine/tree/master/cooling_2009.

We implemented the original model as published by Cooling et al. in full in our own model since we also included NFAT phosphorylation and the de-phosphorylation futile cycle. The entire model as published by Cooling et al. [18] is used in theNK cell model. To implement the model, we first checked the models in PMR forcuration to ensure that the outputs matched the published outputs as described by Cooling et al. [18]. After we satisfied that the model output matched the publishedoutputs, we then incorporated the model into the NK cell signalling pathways.

Implementing novel pathway models (level 2 models)

FCεRIγ appears as Level 2 models in Figure 2. The repository associated with this model can be found at https://github.com/Nurulizza/HLAG_to_cytokine/blob/master/FCepsilonRI.cellml. The simulated Grb2 phosphorylation was a good fit with the experimental observations of Tsang et al. [23]. The model and observed experimental kinetics of phosphorylation of Grb2 are shown in Figure 7. The root mean square (RMS) error for the model is 0.0695 μM. The RMSE is 1.07% of the peak concentration. Visual inspection of the graph confirms this. The best fit to this data set was achieved with the parameters listed in Table 1.

Knowledge of which parameters the model is sensitive to helped to establish which parameters needed to be fixed when we tried to predict to another set of data(eg. the phosphorylation of Grb2). Figures 1 and 2 in Additional File 1 presents the differences in pSyk solutions within the feasible parameter range for all rate constants in this model. We varied each parameter, one at a time, over the feasible parameter range to check how much they affected the solutions while keeping other rate constant parameters fixed.

For forward constants k_{f2}, k_{f4}, k_{f6} and k_{f7}, we observed a minimum in the error corresponding to the fitted parameter value which showed the fitting had convergedto something appropriate where most parameters were very close to at least alocal minimum in the parameter space. It means the model is sensitive to those parameters. The sensitive parameters are the dissociation rate of phosphorylated FCεRIγ and Lyn complex, k_{f2}, association of phosphorylated FCεRIγ and Syk, k_{f4}, association of pSyk and Grb2, k_{f6}, and dissociation of pSyk and Grb2 complex, k_{f7}. These parameters remained fixed in subsequent simulations. Constant forwardrate parameters k_{f1} and reverse rate parameters k_{r1}, k_{r4} and k_{r6} showed distinct changes in model behaviour on one side of the minimum. In this case we can vary these parameters during fitting to another set of data in the range around the minimum in which the line is flat. A flat line was found for k_{f1} and Pi showing that the model is not sensitive to those parameters (data not shown). The latter two types of parameter could therefore be varied over the whole defined range in fitting to subsequent data sets.

Parameter fitting was then performed by fixing the parameters that the previous fitted model was sensitive to: we fixed the value of k_{f2}, k_{f4} k_{f6} and k_{f7} (see Table2). In this subsequent fitting, for constant forward rate parameters k_{f1} and reverse rate parameters k_{r1}, k_{r4} and k_{r6} that showed distinct changes in model behaviouron one side of the minimum, we varied the parameters only over the range thatmodel predictions for the Tsang data were not sensitive to these parameters. Thelist of kinetic rate constants that we are going to fit and the boundaries are givenin Table 3.

The best fit was achieved with the parameters listed in Table 4. The model and the observed experimental [24] kinetics of phosphorylation of FC and Syk are shown in Figure 8. The RMSEs are 0.0089 μM for FC phosphorylation and 0.0022 μM for Syk phosphorylation. These RMS errors are approximately 10% of the peak values for pFC and pSyk. Along with Figure 8 these best fits are not perfect representations of

the data, however, the available data are relatively sparse in time, and appear to contain more noise, so it may not be possible to obtain a clearly better fit to these data points.

However, the model predictions shown in Figure 8 does not predict the experimentally observed drop in pSyk after 1000 s due to formation of pSyk-Grb2 complex. This may be because the concentration of Grb2 in the model was low (0.01 μM), which limited its impact on pSyk. The initial condition of Grb2 was fitted at 0.01 μM to get a good fit to the experimental data. The parameters for FCεRIγ model fitted to data set from Tsang et al. [23] and Faeder et al. [24] are listed in Table 5.The sensitivity analysis of the model is provided in Additional File 2.

The sensitivity analysis showed that the model fitted to the data measured by Faeder et al. [24] is sensitive to the dissociation rate of phosphorylated FCεRIγ and Lyn complex, k_{f2}, the phosphorylation rate of Lyn, k_{f3} and Pi for the pFC. The same parameters especially k_{f3} and Pi, however, do not contribute to pSyk variability. The model fitted the experimental data well with large values of parameters k_{f1}, k_{f4} and k_{f5}. Sensitivity analysis showed that the model converges toward minimum error for both FC and Syk phosphorylation on the right region ofthe parameter space. In contrast, parameters k_{r1} gave the best fit with small valueswhen the model converges toward minimum error for both FC and Syk phosphorylation on the left region of the parameter space. The pathway can be calibratedaround the regions within the minimum error of parameters space. The model wasnot sensitive to the dissociation rate of pFC and Syk, k_{r4}, association of pSyk and Grb2, k_{f6}, dissociation of pSyk and Grb2, k_{r6} and phosphorylation of Grb2, k_{f7} (data not shown). Those parameters are therefore free to be varied in calibration of subsequent components of the model that incorporate this pathway.

Lyn kinase phosphorylates FCεRIγ into phosphorylated FC. Re-phosphorylation of Lyn then occurs. Due to a lack of quantitative information about the aggregationrate of FCεRIγ in the literature, we constructed a simple model of the system, in which we assumed that the FCεRIγ was in the aggregation state. The model neglects aspects of the complex dynamics of the FCεRIγ system, which has previously been incorporated

into mathematical descriptions. This means, that although it capturesthe dynamics of the available experimental data adequately, it may be shown in thefuture to neglect important dynamics, as more experimental data becomes available. The modular structure of this modelling approach would allow the component of the model to be replaced with a more detailed morel in the future, if necessary.

Phosphorylated FCεRIγ activates Syk through binding activity. The activation of Syk eliminates the lag phase in Syk activity and results in a linear rate of Grb2 phosphorylation, indicating that FCεRIγ binding activates Syk. Observations using the model displayed qualitatively similar pFC-Syk binding behaviour to the available experimental data.

Experimental work by Tsang et al. [23] showed that Syk is an OR-gate switch, meaning that it can reach full activation either by ITAM binding or autophosphorylation activation. Tsang et al. demonstrated that activation by both stimuli works through the same mechanism and the application of both stimuli is expected to giveonly a small increase in activity. Our model supports this and implies that ITAM binding is sufficient to cause full activation of Syk. Phosphorylated Syk sustains activity over time to facilitate longer-term changes in cell signalling.

In our model, the Syk is an OR-gate switch, meaning that it can reach full activation with one factor by ITAM binding. The ability of Syk to reach full activationwith a single stimulus helps to define the ability of Syk to sustain its activity over time although after transient activation of ITAM to facilitate longer-term changes in cell signalling. As an example, Syk activity is required for more than 1 hour to induce activation of NFAT transcription [23].

Phosphorylation of Grb2 is dependent on the available concentration of Syk and Grb2 in the cell. The simulation results showed that the model could produce quantitatively similar kinetic behaviour in the phosphorylation of Grb2 to the experimental data. Phosphorylation of Grb2 was initially linear with time and then plateauedafter all the Grb2 was completely phosphorylated. The lag in the reaction time waseliminated.

In conclusion, a minimal FCεRIγ model was developed and implemented in CellML. The results for phosphorylation of Grb2 for a data set from Tsang etal.

[23] were presented to validate and test for phosphorylation of FCε and Syk in a data set from Faeder et al. [24]. A basic sensitivity analysis was performed to study the effect of the model constants' parameters on the model.

HLA-G cytokines model

This section introduces the model labelled HLA-G cytokines in Figure 2. The respository associated with this model can be found at https://github.com/Nurulizza/HLAG_to_cytokine. The fit of the model to the experimental data shown in Figure 9. The simulated cytokine output showed similar behaviour for IFNγ secretion as the experiment. The model did not fit as well to TNFα secretion as shown in the figure. With the limitation of knowledge and data on the pathway inside the nucleus, we simplified the pathway by assuming the cytokine secretion is proportional to the NFAT translocation into the nucleus. In the model, the production of IFNγ and TNFα are k_{f4} and k_{f5}.

The sensitivity analysis shows that IFNγ and TNFα productions are sensitive to both parameters, meaning that the changes of any parameter will affect the secretion of both cytokines. To elevate the secretion of TNFα at 8,000 s causes bad fit to IFNγ secretions. In this multi-objective optimisation, the model was only able to represent the IFNγ data accurately. When more data become available in the future, especially the knowledge of signalling pathway inside the nucleus, we hope the fitting can be improved. The model, however, captured the delay in cytokine production as expected. The best fit achieved with the parameters listed in Table 6.

The sensitivity analysis of the model is provided in Additional File 3. The sensitivity analysis of the model shows that the model is sensitive to parameters k_{f2}, k_{f21}, k_{f22}, k_{f23} and k_{r21}. The model is also sensitive to parameters k_{f4}, k_{f5} and k_{f31} in component cytokines. The analysis showed that parameters k_{f21} depicts the binding activated calcineurin to $NFATp_c$ to form the complex $NFATN_c$, k_{f21} and the nuclear import rate, k_{f22} are the most sensitive parameters that gave big difference to the model within the tested parameter space, that are between 10^0 and 10^2 and between 10^{-2} and 10^2. Parameters k_{f23} and k_{f2} sit on minimum within the the edge of regions within the tested parameters space. Parameters k_{f5} and k_{f31} are significant to either

the production of IFNγ or TNFα.

Discussion

Here we aimed to model the regulation of activated KIR2DL4 receptor towardsthe production of IFNγ and TNFα cytokines. The activation of the endocytosed KIR2DL4 receptor was stimulated by the binding of soluble HLA-G. The full path- way was fitted to an NK cell dataset from Rajagopalan et al. [25]. As explained earlier, the use of the antibody KIR2DL4-specific involved small differences from natural HLA-G. In the model, we considered a simple case, which adequately catered for the biological understanding of the reactions. The model developed in this study has some limitations. The sub-models are fitted to several types of data. We usedB cell data [23] and RBL data [24] for the FCεRIγ model and data for the pub- lished model by Dupount and Erneux [17] and Cooling et al. [18] were from Chinese hamster ovary cells and myocyte data, respectively.

In this study an ODE model has been employed. As the aim of the study is to capture a large signalling pathway, with significant interconnectivity, this providesthe simple to generate and readily interpretable model of the system. In addition, information on spatial distribution of components of the pathway and data with which to parameterise a stochastic model is limited. However, in the future as databecomes available, it may be possible to derive more complete descriptions of thesystem using these techniques. A J flux for each reaction is defined to simplifythe equation. J flux comprises the concentration of species, and rate constants k_f (forward reaction) and k_r (reverse reaction). The model is encoded in CellML.

The signalling pathway to be modelled, depicted in Figure 2 consist of many components and reactions. To create a monolithic mathematical model which describesall these reactions would lead to a complicated model with many ODEs to solve. To simplify the problem, in this study, the development of the KIR2DL4 intracellular signalling model employs a composite approach for generating modular models.

The approach allows for the construction of large-scale complex model by combining component of sub-models that can be modified separately or individually [26]. The composite modular model brings together a series of sub-models. The sub-modelscan be derived from curated published models or newly developed models.

Hetherington et al. described five advantages of using compositing for the construction of complex system models. The advantages that are related to this study are (i) Increases understanding by presenting a complex system in distinct functional modules. (ii) Each sub-model can be developed separately and non-simultaneously i.e. at different times, and even by different researchers. (iii) A sub-model can be modified without affecting other sub-models. (iv) Sub-models may be re-used for other models. (v) Sub-models may be independently calibrated or tested [26].

A major concern when modelling a biological system is that not all initial conditions and parameters for each activity in a cell are known. Unknown parameter values can be estimated using model calibration or fitting techniques to get valuesthat fit the model behaviour to some experimentally observed behaviour. Model fitting can provide possible parameters that will help to produce reliable computational modelling results. In this study, the model parameter optimisation of CellMLmodels was done using Python inside the OpenCOR tool. Model parameter optimisation to available experimental data helped us to simulate the model and capture experimental outputs.

In general, sensitivity analysis is the study of the changes of optimal solution when there are changes in the constant parameters [27]. A sensitivity analysis was performed to determine the sensitivity of rate constant parameters in the model. Each of these parameters determine changes in the model.

Conclusions

The mathematical model was built based on the qualitative signalling pathway described in the KEGG database. From this qualitative description we built a quantitative model for the pathway, reusing existing curated models where possible andimplementing new models as needed. Using simulations with fitted parameters, themodel outputs increased our current understanding of pbNK intracellular signalling

defining how it reacts to target cells through the activation of receptors. The developed model enabled us to identify key parameters and molecules that influence IFNγ and TNFα cytokine secretions. The mathematical model of the intracellular signalling pathway shed light on processes occurring in the cell that cannot be observed directly through experimental measurements. The model provided a tool to test KIR2DL4 reactions to target cells under different conditions.

The model was built sub-model by sub-model and was fitted against available experimental data. After we were satisfied with the parameter optimisation, we then checked the sensitivity of each parameter in the sub-models. Sensitivity analysis gave us ideas on which parameters affected the model and which parameters could be modified against new data sets. Once we were satisfied that no other data were available to use, we created a KIR2DL4 pathway by modularising the sub-models. The pathway was then fitted to pbNK cell cytokine secretion experimental data published by Rajagopalan et al. [25]. This approach was enabled through the availability of these models in standard formats in publicly accessible repositories. We apply modular design principles into the construction of signalling model.

The model was developed in CellML, which allows for modulation of the model.The model was developed in sub-models. The sub-models were developed so that they can be re-used in a new model, partially or as a whole. Each sub-models was fitted to available experimental data. An important contribution to the stateof knowledge is the free availability of the code base, which makes it possible to independently simulate and to modify or extend the model for different applications.

Methods

Model construction

To identify appropriate signalling pathways to derive models at all levels and mod-els that had been previously published that covered components of the system we used online databases as resources for signalling pathway and experimentaldata. KEGG (https://www.genome.jp/kegg/pathway.html) is the main sourcefor cell signalling pathways. Several model repositories of computational models of biological processes were searched for existing models. The databases searched

included PMR (https://models.physiomeproject.org/welcome) and BioModels (https://www.ebi.ac.uk/biomodels-main/), where the first is the CellML model

repository and the latter is the SBML model repository. The models in those repositories are published in either curated and non-curated form. We also extended the data search into the JWS Model Database (http://jjj.biochem.sun.ac.za/), an online modelling database that allows online simulation of models. Models described in the literature were manually curated and enriched with cross-references.

Re-using components of existing model in CellML

To re-use an existing model, we first re-simulated the model to ensure the model outputs were the same as published outputs. We then imported component/s or variable/s that we intended to re-use in our model. We then encapsulated the components. The steps in re-using and importing components from existing models to a new top-level model are shown in simplified form in a flow chart provided in Additional File 4.

The new model is usually a top level model, which may contain the CellML sub-model(s) imports, the encapsulation hierarchy, and the units, components and mappings of the new model. The top-level model and sub-models are linked using public mapping and private-public mapping if encapsulation is used. The CellML model of a top level model with sub-model(s) imports is provided in Additional File 5. We then tested the model to ensure it worked as expected.

Methods for searching for experimental data

Several methods were used to gain information for the experimental data in this study. Various keywords for data searches were used, ranging from general to specific terms, and combinations of both vague and specific keywords. The data search was done for NK cell signalling experimental output, and for the signalling experimental output for other immune cells including T cells, B cells and macrophages. We extended the data search to other non-immune cell types to ensure we obtained all available data. But we tried to make use of data from immune cells first. The search keywords included single molecule keywords such as HLA, KIR, PI3K, and Vav. We also used combinations including trophoblast-NK cell, receptor-ligand combinations, receptor-cytokine combinations,

receptor/ligand-molecule combinations, molecule-molecule combinations, molecule-cytokine combinations. Other keywords were used to search for specific signalling pathways, such as MAPK, NFAT futile cycle and calcium oscillation.

We also referred to the Protein Data Bank (PDB) (https://www.rcsb.org/), a database for three-dimensional structural data for large biological molecules, such as proteins and nucleic acids, for annotated collections of publicly available molecular structures, using relevant data such as molecular weight. Large amounts of additional relevant data are available through databases such as the Gene Expression Atlas (https://www.ebi.ac.uk/gxa/home), which is an open resource database that provides a huge quantity of information about gene and protein expression. The data relevant to signalling pathways that we could access in this databasedealt with the relative expression of genes.

Once a model has been developed, enough experimental data is crucial to ensurethat the *in silico* simulation is reliable. The data sources can vary from journals to laboratory findings from experiments. Our model incorporated a wide variety of empirical observations ranging from human to non-human primates. Data that we needed included initial conditions of species involved in the pathway and kinetic rates of reactions. We examined literature data including integrative pathway diagrams, quantitative and qualitative details of possible molecular states, interaction and activities [28]. Appropriate parameter values were chosen from the literature where possible and others were optimised using parameter fitting.

Initial conditions

In this study, the initial conditions for substrates were derived from literature where possible. The initial conditions depend on the experiment conducted, or be fit if unknown. For experimental data that using the same unit, the value can be used directly. In some circumstance, experimental data was generated in different unit tothe model, i.e. pg/ml, so the data need to be converted to molarity using a formula as follows

$$\textit{Molar concentration, } c_i = \frac{P_i}{M_i}\, c_i$$

where p is the density of constituent i, and M is the molar mass of constituent.

For substrate without any data, we used the relative initial condition that has been optimised for similar reaction or we made early assumption within the relevantrange. Once we optimised the model, we then decide whether we need to increaseor decrease the value. The complexes in the system were fixed at 0 uM at time t=0.

Model calibration (parameter estimation)

Parameter estimation is a widely used method to estimate unknown parametersfor mathematical models [29]. Most of the time, experimental data can't be used directly in a mathematical model due to many reasons, i.e. different experimental condition and measurement unit. Gutenkunst et al. highlighted that parameter estimation is complicated because of large measurement error and the model be- haviour also often insensitive to changes of an individual or combined parameter values [29, 30].

Here we address the parameter estimation using least-squares optimisation in Python. The parameter estimation implements the Levenburg-Marquardt gradient method (greedy algorithm) to minimise an objective function [31]. The first step isto define the objective function to minimise. Gradient methods such as Levenburg-Marquardt tend to run into the nearest local minimum. The method is also sensitiveto initialisation of parameters to be fit. The algorithm iteratively solves a trust- region sub-problems augmented by a special diagonal quadratic term and with trust-region shape determined by the distance from the bounds and the directionof the gradient. This enhancements help to avoid making steps directly into bounds and efficiently explore the whole space of variables. Traditional gradient-based local optimization methods normally fail to get to a global minimum.

As the least-square method is prone to finding a local minimum rather thana global minimum [32, 33], it is important to be reasonably close to the global minimum to get the best fit. To surmount this limitation, we must conduct a sweepof parameter space to find suitable search regions [34]. However, for many of our models, there are several unknown parameters, and so parameter space is too largeto practically cover simply by varying parameters one by one. We therefore, aim torandomly sample

parameter space with suitable coverage to be able to assure that we can find solutions close to a global minimum [35]. We use a sampling methodto create a random sample of parameters within identified boundaries [36, 37, 38].It allows users to determine the sampling size where the big sample size gives morechance for a better fit. It then runs the model lots of times using sampled parameterspace and ranks the parameter set by the objective function. The parameter sampleswere generated using the Saltelli sample function stored in Python modules [36, 37,38] as following

$$N \times (2D + 2)$$

where N is the scaling factor of samples to generate (the argument we supplied) and D is the number of model parameters. Parameter sweep generates samples within the specified parameter space.

We then generally loop over each sample input and evaluate the model. The parameter fitting was conducted via the optimisation of objective function. The objective function was defined as the sum of the squared differences between predicted and experimental values. The equation is defined as

$$S = \sum_{i=1}^{n} (x_i - \bar{x})^2 n$$

where S is the sum of the squared differences between experimental and predicted values.

The unknown parameters may cover orders of magnitude, so we need to cover solutions, equally and fairly over a large parameter sweep. For this reason the fitting assumes exponents for parameter bounds. For example a lower bound of -3 and an upper bound of 2 will sweep parameters between 10^{-3} and 10^{2}.

Parameter estimation aims to find the possible parameters that minimise the difference between the model output and experimental data. We can measure how good is the fit by looking at the error value, where the lower error value means

better fitting. We also can compare the graph between prediction and experimentaldata visually.

In this study, we used the default tolerance for termination by the change of the cost function and termination by the change of the independent variables. Default value set by the leastsq for both tolerances is 1e-8. The lower and upper bounds on independent variables are also set for each parameter.

Model analysis (sensitivity analysis)

Model uncertainty often has done as an analysis that is carried out after model construction and calibration have been completed [39]. One of the methodologies for uncertainty assessment is sensitivity analysis [39]. Sensitivity analysis is the studyof how the inputs of a given model can change solution or output of the model, particularly of how the different level in the input of a model can be qualitatively or quantitatively apportioned to different outputs of a model [39, 35, 40]. One of the limitations of sensitivity analysis is the tendency to takes the model structure and system boundaries for granted [41].

There are many types of sensitivity analysis methods that can be used to access model uncertainty. For example, the quantitative variance-based methods, global sensitivity with regional properties [41], and the simplest class of the one factor ata time (OAT) screening techniques, which simply vary one factor at a time and measure the variation in the output [41]. Some form of various global sensitivity methods has been described in a few publications [35, 42, 43, 44]. Ratto et al. (2001) have demonstrated how different methods like Sobol indices, FAST, correlation matrix or principal component analysis (PCA) can be used to achieve a better understanding of parameter sensitivity [44, 45].

The drawback of developing a big model in a small compartment is that the non-sensitive parameter from the small sub-model can be inherited to the bigger sub-model. Sensitivity analysis is one of the methods to access uncertainty in modelparameter and can be used to identify parameter that need to be quantified experimentally.

To perform the analysis to NK cell model, each sub-model was analysed by lookingat how sensitive is the model to each involved parameter. For small sub-models weuse the one parameter at a time approach. That is, we change one parameter ata time and keep the other parameters fixed and investigate how that parameter impacts the objective function error. We initialised the model with the best fit values for each parameter, and ran it multiple times over the parameter range. Wevaried each parameter from its best fit value,

over the parameter range we assumed it to take. The analysis is repeated for all the parameters. We vary parameters overthe feasible parameter range to check how much they impact solutions.

Error defines the differences between points in model solution and experimentalsolution. In this study, we used least-squares method which calculated the sum of the squared points of model from data. We plot a graph of the error (shown on they-axis) versus parameter range (shown on the y-axis). Dips in the error correspondto local minima in the parameter space. If a model is sensitive to a parameter,it remained fixed in subsequent simulations. At times the mimimum was right at the edge of the parameter space. This parameter showed distinct changes in model behaviour on one side of the minimum can be varied during fitting to another set of data in the range around the minimum in which the line is flat. This means this parameter value needs to be around the 'minimum'. A flat line showed that the model is not sensitive to those parameters. The latter two types of parameter can be varied in fitting to subsequent data sets.

Modelling intracellular signalling of HLA-G-KIR2DL4 pathway

Re-using and implementing models from Physiome Model Repository (level 1models)

The Ca^{2+} model. Effects of inositol 1, 4, 5-trisphosphate 3-kinase and 5-phosphataseactivities on Ca^{2+} oscillations

This section outlines the model labelled as Ca^{2+} sub-model in Figure 2. Dupont and Erneux simulated a model that capturesthe oscillation of Ca^{2+} in a cell in response to upstream signalling (Figure 3) [17]. We implemented the Ca^{2+} oscillations phenomenon from Dupont & Erneux, 1997 in our model (https://github.com/Nurulizza/HLAG_to_cytokine/tree/master/dupont_1997).

This model describes the link between activation of phospholipase C (Plc) and Ca2+ dynamics in the cell. IP3 activates the release of Ca^{2+} from internal stores via IP3 receptors. The model simulation showed that IP3 and IP4 oscillations are passively controlled by the cytosolic Ca^{2+} oscillations. The oscillations are caused by feedback regulation of cytosolic Ca^{2+} on the IP3 receptor.

The concentration of cytosolic Ca^{2+} is given by the following equation

$$\frac{d[C_{cyto}]}{dx} = k_1(b + I_{ra})\left(Ca_{tot} - C_{cyto}(\alpha + 1)\right) - V_{MP}\frac{C_{cyto}^{n_p}}{K_p^{n_p} + C_{cyto}^{n_p}}$$

where C_{cyto} and Ca_{tot} are the concentration of cytosolic Ca^{2+} and total Ca^{2+}. k_{1b} describes the kinetic rate of Ca^{2+} from the stores into the cytosol, I_{ra} is the fraction of active channels. α represents the ratio between the volumes of the in- tracellular stores and the cytosol and b accounts for a basal efflux from the stores into the cytosol. Translocation of Ca^{2+} back to stores is controlled by cytosolic Ca^{2+}, described using the Hill approximation where V_{MP}, K_p and n_p describe the maximum velocity, the constant for half maximum activity, and the Hill coefficient,respectively.

In this model, Dupont and Erneux observed the typical behaviour of cytosolic Ca^{2+} oscillations and the influence of Ca^{2+} oscillation on the oscillation of IP3 and IP4 concentrations. This happens because each Ca^{2+} spike activates IP3 3-kinase, which further stimulates the change of IP3 into IP4. The amplitudes of IP3 and IP4are determined by the stimulation level and by the maximum velocity and thresholdconstant of the IP3 3-kinase. The model was verified against the paper.

The NFAT model. Sensitivity of NFAT cycling to cytosolic calcium concentration.

This section describes the model labelled as 'NFAT' in Figure 2. The nuclear factor of activated T-cell (NFAT) transcription factors is stimulated by calcium signals.In our model, the activation of NFAT is also stimulated by calcium. In NK cell, the activation and translocation of NFAT into the nucleus stimulate the production of cytokines. In 2009, Cooling et al. [18] simulated NFAT activation and translocation to the cell nucleus to regulate gene transcription. They replicated important regulation of calcium Ca^{2+} oscillations and calcineurin (CaN) to downstream NFAT cycling. We implemented Cooling et al.'s 2009 model [18] in our model, which includes the same pathway (https://github.com/Nurulizza/HLAG_to_cytokine/tree/master/cooling_2009).

The IP3-Ca^{2+}-CaN pathway plays an important role in the stimulation of transcription factor NFAT [18]. Signals from upstream Ca^{2+}-CaN dephosphorylate NFAT in the cytoplasm. During dephosphorylation, NFAT is translocated into the nucleus. In the NFAT cycling model built by Cooling, Ca^{2+} activates calmodulin-calcineurin complex (calmodulin is not shown in Figure 5 as it forms complex with CaN), which further binds to NFAT and dephosphorylates it in the cytosol. The dephosphorylated NFAT translocates to the nucleus. NFAT may also be rephosphorylated and translocated back to the cytosol.

In this model, calcineurin is activated by calcium (Ca). Activated calcineurin thendephosphorylates NFAT. The dephosphorylation of NFAT allows the translocationof NFAT to the cell nucleus. In this model, we assumed that NFAT can be rephosphorylated by a number of kinases. Once NFAT is rephosphorylated, it is exportedback to the cytoplasm.

The model has six unknown parameters, which were fitted to data from baby hamster kidney (BHK) cells. The model implements an approach defined by Tomida et al. [22] to investigate calcium effects in BHK cells. The outputs from themodel show that an oscillating calcium signal is more efficient than a constant calcium signal. The size of the calcium signal determines the NFAT cycling rate. The implementation of this model allows us to replicate Ca^{2+} mobilization in NK cells. The model also simulated the dephosphorylation of NFAT in the cytosol. From their model, they also found out that the dephosphorylated NFAT in the cytosol isbuffered before declining. Nuclear NFAT was observed to rise steadily, as seen in theexperimental data. The model was also able to replicate the effect of overexpressionof calcineurin on the NFAT cycle. The model showed a normal NFAT cycle withoverexpressed calcineurin at the same time that calcium is set at a constant level. Inour cell signalling, the translocation of NFAT into the cell nucleus leads to secretion of cytotokines.

To simplify the model, as in the original publication [18], NFAT phosphorylationand dephosphorylation reactions are modelled as single steps, although in nature there is more than one phosphorylation site involved. The model also assumed a single step for NFAT translocation. The NFAT translocations into and from the nucleus do not have back reactions. This process is described using a futile cycle inthe system.

With these assumptions, the phosphorylation and dephosphorylation of NFAT, together with translocations of NFAT into and from the nucleus, are described using mass action kinetics. The phosphorylation and dephosphorylation are described as

$$NFATp_c + N_{active} \Leftrightarrow NFATN_c,$$

$$J_1 = k_{f1} \times NFAT_{pC} \times N_{tot} \times act_N \times -k_{r1} \times NFATN_c \times (1 - act_N),$$

where N_{active} is the amount of activated calcineurin, determined by the total calcineurin, N_{tot} and fraction of activated calcineurin, Act_N.
Thus, the translocations of NFAT into and from the nucleus are described as

$$NFATNp_n \rightarrow NFATp_c,$$

$$J_2 = NFATN_c \times k_{f2},$$

$$NFATN_c \rightarrow NFATN_n,$$

$$J_4 = NFATp_n \times k_{f4}.$$

Parameter fitting was performed against the data of Tomida et al. [22], by Cooling [18] and the model was verified against the paper.

Implementing novel pathway models (level 2 models)

A new sub-model that was built to complete the whole signalling pathway, based onthe availability of experimental data. One sub-model was developed in this sectionand termed $FC\varepsilon RI\gamma$ and appear as Level 2 models in Figure 2. The repository associated with this model can be found at https://github.com/Nurulizza/HLAG_to_cytokine/blob/master/FCepsilonRI.cellml. Two sets of experimental data were available in the literature for this pathway. One was published by Tsang et

al. (2008) [23] and the other by Faeder et al. (2003) [24]. This model was built basedon data from both literature. Previously Faeder et al. developed a model of early signalling of $FC\varepsilon RI\gamma$ (FCε) [24], however, this model was focussed on the receptor itself and contained a greater level of complexity than was required in our model. Inthis sub-model we aimed to build a simple model of signalling of FCε that still rep- resented biological understanding and fitted the experimental data (Figure 6). FCε exists in tetrameric form, which has an α-chain, a β-chain and two disulfide-linkedγ-chain [24]. The α subunit can be bound to ligand or unbound, a β-chain has fourpossible states of phosphorylation and two disulfide-linked γ-chain has six states of phosphorylations. In total, there are 300 possible states of receptor subunits for FCε [24]. To avoid complexity, we assumed that FCε is in an aggregated state and ready for binding with other reactants. The activated FCε receptor is transphosphorylated by pLyn, available at the cell surface. This followed by the recruitment of Syk to the membrane surface which is subsequently transautophosphorylated by phosphorylated FC*E*. Inactive Grb2 then binds to phosphorylated Syk, and becomes phosphorylated.

Syk is a tyrosine kinase that is important in bridging receptor ligation and down-stream signalling such as Ca^{2+} and MAPK. Once the cell receptor binds with the ligand, $FC\varepsilon RI\gamma$ (ITAM receptor) is recruited and transphosphorylated by Lyn. The phosphorylated ITAM then recruits protein tyrosine kinase (Syk). Previous studies have shown that ITAM phosphorylation increases Syk activity and modulates Syk potency [23]. It must be noted that concentration above 10 μM ITAM can inhibit Syk activity [23]. Phosphorylated Syk then phosphorylates Grb2 (growth-factor- receptor-bound protein 2). Phosphorylation of Grb2 leads to the activation of PI3K downstream signalling. To match the available experimental data, we assumed thatthe Lyn kinase is rephosphorylated for recruitment of additional pLyn into the system to ensure that the system has enough supply of phosphorylated Lyn. The equation associated with this reaction is

$$Lyn + Pi \xrightarrow{k_3} pLyn$$

where Pi denoted a phosphate, k denotes a forward reaction and pLyn denotes a phosphorylated Lyn.

The flux associated with this reaction is

$$J3 = k_3[Pi][Lyn],$$

where J denotes a flux, k denotes kinetic constant and Pi denotes a phosphate.

Experimental detail on Syk activity in B cells is presented in the study by Tsang et al. [23] which captures the molecular mechanism of Syk activation in vitro. The studies explore Syk activity under various conditions: activities of phosphorylated and non-phosphorylated Syk; activation of Syk by different receptors; and whether or not Syk is an OR-gate type of molecular switch. Syk activity is required for more than one hour to induce activation of downstream reactions, so the experiment was run for 3600 s. For that reason, the model simulation time was set for 3600 s. For the FCε model, we had 10 unknown parameters to fit to this data.

In one of the observations, Tsang looked at the activity of Syk when bound to FCεRIγ. The experimental data we fitted the model to were for a temporal Grb2 phosphorylation by dephosphorylated Syk with 1 μM FCεRIγ. The Syk concentration used in the experiment was 0.005 μM. Experimental data points were digitised from Supplemental Figure 2 in Tsang et al. [23]. The observed experimental data points were from spectrophotometrical measurements of phosphorylation in a single representative experiment [23]. The binding of Syk to the receptor eliminated the lag phase in Grb2 phosphorylation.

The second data set was adapted from Faeder et al. [24]. In their simulation, Faeder et al. looked at the pathway in rat basophilic leukemia (RBL) cells. The experimental environment was maintained at a temperature of 27°C. The cell density and cell volume were assumed to be 1×10^6 cells/ml and 1.4×10^9 ml. The observed experimental data points were from densitometric measurements of phosphorylation in a single representative experiment [24, 46]. Experimental data points were digitised from Figures 3(b) and 3(d) in Faeder et al. [24].

Parameter estimation was performed with each unknown kinetic rate constant allowed to vary in a feasible range that is between 1×10^{-3} and 1×10^2 [47]. However, we expand the range when we see the optimisation error potentially decreasing with larger boundary. The settings for this work are described in Table 7. We estimated the concentration of Grb2 and pLyn at 6.47 μM and 6.5 μM. The phosphorylated (except Lyn) and complex reactants are assumed to be 0 at time 0 s. The number of sample used for the fitting is 500 which generate 12000 samples.

Tsang and Faeder used different experimental protocols so the initial conditions in our

model representing these protocols differed. To fit the model to data from Faeder, some initial conditions were derived from the experimental protocol re- ported, and others were estimated during model fitting. We fitted concentration of FCεRIγ is 0.0474 μM, the concentration of Syk is 0.025 μM, and the concentration of pLyn is 0.0474 μM. The list of initial conditions is listed in Table 8.

Modularisation of sub-models toward a complete HLA-G-KIRDL4 pathway

This section introduces the model labelled HLA-G cytokines in Figure 2. The respository associated with this model can be found at https://github.com/Nurulizza/HLAG_to_cytokine. Experimental studies by Rajagopalan et al. [25] observed the activation of KIR2DL4 by soluble HLA-G. The authors also suggest that the activation of uNK cells promotes a proinflammatory/proangiogenis response in uNKcells, which further promotes enlargement of blood vessels in early pregnancy [25]. Soluble HLA-G has been known to be a ligand for 2DL4. Soluble HLA-G originates from cell surface-bound HLA-G. Metalloproteinase (a protease enzyme) isresponsible for the cleavage/release of HLA-G from the surface. The experimentalsetting used to fit the data also used soluble HLA-G to stimulate KIR2DL4. In our model, we assumed that the HLA-G that binds to KIR2DL4 is soluble HLA-G.

The transient passage of endocytosed KIR2DL4 receptor at the cell surface occurswhen an NK cell is activated by IL-2 is sufficient to capture soluble HLA-G and transport it to the endosomes. The endocytosed HLA-G/KIR2DL4 complex recruits FCεRIγ and aggregate FCε. FCεRIγ activation is known to induce phosphoinositide 3-kinase (PI3K) [48, 49]. PI3K-mediated production of phosphatidylinositol 3,4,5- triphosphate (PtdIns(3,4,5)P3) allosterically enhances PLCγ activity downstream. This early signalling pathway then activates the NFAT futile cycle and initiates theregulation of IFNγ and TNFα secretion in NK cells.

The endocytosed HLA-G/KIR2DL4 complex recruits FCεRIγ and aggregates FC. FCεRIγ activation is also known to induce phosphoinositide 3-kinase (PI3K) [48, 49]. PI3K-mediated production of phosphatidylinositol 3,4,5-triphosphate (Pt-dIns(3,4,5)P3) allosterically enhances PLCγ activity downstream. This early signalling pathway then activates the NFAT futile cycle and initiates the regulation ofIFNγ and TNFα secretion in NK cells.

Our model replicates the reaction of NK cells stimulated by KIR2DL4-specific antibody.

However, stimulation by the natural ligand, HLA-G, showed a quantitatively similar cytokine response. For most of the secreted cytokines, natural HLA-G induced at least 50% of the amount induced by antiKIR2DL4 mAb [25]. In the experiment, the secretion of TNFα was detected within the first 2 hours and up- regulated more than 2-fold. The secretion of IFNγ was upregulated 1.5-fold after 8hours of receptor activation.

This large pathway is integrated by three level 1 and level 2 sub-models. Two ofthe sub-models are published sub-models: the Ca^{2+} model (labelled Ca^{2+} in Figure 2) [17] and the NFAT model (labelled NFAT in Figure 2) [18]. This pathway also includes the FCεRIγ model (labelled FCεRIγ in Figure 2).

Two short reactions needed to be added to the model to connect componentsof the system. These are a representation of the HLA-G activation and the NFAT cytokines. The first reaction describes the activation of KIR2DL4 by HLA-G. The second reaction describes the secretion of IFNγ and TNFα through activation of NFAT downstream in this pathway.

The reactions that correspond to this portion of the signalling pathway are

$$hG + 2DL4 \underset{k_{-10}}{\overset{k_{10}}{\Longleftrightarrow}} hG2DL4$$

$$hG2DL4 + FC \underset{k_{-1}}{\overset{k_{1}}{\Longleftrightarrow}} hG2DL4FC$$

The fluxes associated with these reactions are

$$J10 = k_{10}[hG][2DL4] - k_{-10}[hG2DL4]$$

$$J1 = k_1[hG2DL4][FC] - k_{-1}[hG2DL4FC].$$

Cytokine produces by a cell will be used for cell regulation. Although the modelonly captures the production of cytokine inside the cell, we added cytokines released from the cell that is applicable to all cytokines. We, therefore, added reactions for cytokine release for both TNFα and IFNγ.

The reactions associated with the reactions are

$$TNF\alpha \xrightarrow{k_{31}} TNF\alpha \qquad released,$$

$$IFN\gamma \xrightarrow{k_{32}} IFN\,\gamma \qquad released.$$

Parameter fitting was performed using experimental data by Rajagopalan et al. [25]. Each unknown kinetic rate constant varies differently and the boundaries usedfor the fitting process are listed in Table 9. At this point, we fixed the initial conditions and kinetic rate constants estimated in individual published sub-models. However, we fitted parameters that were not sensitive to FCε model.

We applied initial conditions as observed by Rajagopalan et al. [25] for HLA-G and KIR2Dl4. The initial conditions for HLA-G and KIR2Dl4 were set at 0.098 μMand 0.1052 μM, respectively. The initial conditions for PI3K was set at 0.01 μM. As shown by the reaction equation above, we assumed that the production of IFNγ and TNFα secretion were parallel to NFAT de-phosphorylation in the nucleus. We estimated the initial condition for plc (non-activated plc) was 1.3 μM, consisent with the initial condition for activated plc. The list of initial conditions adoptedfrom the experiment for the HLA-G activation model, NFAT cytokines model and PI3K activation are shown in Table 10. In this model, we fitted 13 kinetic parameters including 5 parameters from the FCε model.

References

1. Vivier, E., Nunès, J.A., Vély, F.: Natural killer cell signaling pathways. Science **306**(5701), 1517–1519 (2004)
2. Höglund, P., Brodin, P.: Current perspectives of natural killer cell education by mhc class i molecules. Nature Reviews Immunology **10**(10), 724–734 (2010)
3. Vivier, E., Raulet, D.H., Moretta, A., Caligiuri, M.A., Zitvogel, L., Lanier, L.L., Yokoyama, W.M., Ugolini, S.: Innate or adaptive immunity? the example of natural killer cells. Science **331**(6013), 44–49 (2011)
4. Cooper, M.A., Fehniger, T.A., Caligiuri, M.A.: The biology of human natural killer-cell subsets. Trends inimmunology **22**(11), 633–640 (2001)
5. Mace, E.M., Dongre, P., Hsu, H.-T., Sinha, P., James, A.M., Mann, S.S., Forbes, L.R., Watkin, L.B., Orange, J.S.: Cell biological steps and checkpoints in accessing nk cell cytotoxicity. Immunology and cell biology **92**(3), 245–255 (2014)
6. Middleton, D., Gonzelez, F.: The extensive polymorphism of kir genes. Immunology **129**(1), 8–19 (2010)
7. Biron, C.A., Nguyen, K.B., Pien, G.C., Cousens, L.P., Salazar-Mather, T.P.: Natural killer cells in antiviral defense: function and regulation by innate cytokines. Annual review of immunology **17**(1), 189–220 (1999)
8. Scott, P., Trinchieri, G.: The role of natural killer cells in host—parasite interactions. Current opinion inimmunology **7**(1), 34–40 (1995)
9. Long, E.O., Sik Kim, H., Liu, D., Peterson, M.E., Rajagopalan, S.: Controlling natural killer cell responses: integration of signals for activation and inhibition. Annual review of immunology **31**, 227–258 (2013)
10. Cooper, M.A., Fehniger, T.A., Turner, S.C., Chen, K.S., Ghaheri, B.A., Ghayur, T., Carson, W.E., Caligiuri, M.A.: Human natural killer cells: a unique innate immunoregulatory role for the cd56bright subset. Blood **97**(10), 3146–3151 (2001)
11. Bryceson, Y.T., March, M.E., Ljunggren, H.-G., Long, E.O.: Activation, coactivation, and costimulation ofresting human natural killer cells. Immunological reviews **214**(1), 73–91 (2006)
12. Smyth, M.J., Cretney, E., Kelly, J.M., Westwood, J.A., Street, S.E., Yagita, H., Takeda, K., van Dommelen, S.L., Degli-Esposti, M.A., Hayakawa, Y.: Activation of nk cell cytotoxicity.

Molecular immunology **42**(4), 501–510 (2005)

13. Azzoni, L., Kamoun, M., Salcedo, T.W., Kanakaraj, P., Perussia, B.: Stimulation of fc gamma riiia results in phospholipase c-gamma 1 tyrosine phosphorylation and p56lck activation. Journal of Experimental Medicine **176**(6), 1745–1750 (1992)
14. Ting, A.T., Karnitz, L.M., Schoon, R.A., Abraham, R.T., Leibson, P.J.: Fc gamma receptor activation induces the tyrosine phosphorylation of both phospholipase c (plc)-gamma 1 and plc-gamma 2 in natural killer cells. Journal of Experimental Medicine **176**(6), 1751–1755 (1992)
15. Aramburu, J., Azzoni, L., Rao, A., Perussia, B.: Activation and expression of the nuclear factors of activated t cells, nfatp and nfatc, in human natural killer cells: regulation upon cd16 ligand binding. Journal of Experimental Medicine **182**(3), 801–810 (1995)
16. Sica, A., Dorman, L., Viggiano, V., Cippitelli, M., Ghosh, P., Rice, N., Young, H.A.: Interaction of nf-κb and nfat with the interferon-γ promoter. Journal of Biological Chemistry **272**(48), 30412–30420 (1997)
17. Dupont, G., Erneux, C.: Simulations of the effects of inositol 1, 4, 5-trisphosphate 3-kinase and 5-phosphatase activities on ca2+ oscillations. Cell calcium **22**(5), 321–331 (1997)
18. Cooling, M.T., Hunter, P., Crampin, E.J.: Sensitivity of nfat cycling to cytosolic calcium concentration: implications for hypertrophic signals in cardiac myocytes. Biophysical journal **96**(6), 2095–2104 (2009)
19. Dupont, G., Combettes, L., Bird, G.S., Putney, J.W.: Calcium oscillations. Cold Spring Harbor perspectives in biology **3**(3), 004226 (2011)
20. Dolmetsch, R.E., Xu, K., Lewis, R.S.: Calcium oscillations increase the efficiency and specificity of gene expression. Nature **392**(6679), 933 (1998)
21. Launay, P., Cheng, H., Srivatsan, S., Penner, R., Fleig, A., Kinet, J.-P.: Trpm4 regulates calcium oscillations after t cell activation. Science **306**(5700), 1374–1377 (2004)
22. Tomida, T., Hirose, K., Takizawa, A., Shibasaki, F., Iino, M.: Nfat functions as a working memory of ca2+ signals in decoding ca2+ oscillation. The EMBO journal **22**(15), 3825–3832 (2003)
23. Tsang, E., Giannetti, A.M., Shaw, D., Dinh, M., Joyce, K., Gandhi, S., Ho, H., Wang, S., Papp, E., Bradshaw, J.M.: Molecular mechanism of the syk activation switch. Journal of Biological Chemistry **283**(47), 32650–32659 (2008)
24. Faeder, J.R., Hlavacek, W.S., Reischl, I., Blinov, M.L., Metzger, H., Redondo, A., Wofsy, C.,

Goldstein, B.: Investigation of early events in fcεri-mediated signaling using a detailed mathematical model. The Journal of Immunology **170**(7), 3769–3781 (2003)

25. Rajagopalan, S., Bryceson, Y.T., Kuppusamy, S.P., Geraghty, D.E., van der Meer, A., Joosten, I., Long, E.O.: Activation of nk cells by an endocytosed receptor for soluble hla-g. PLoS biology **4**(1), 9 (2005)
26. Hetherington, J., Sumner, T., Seymour, R., Li, L., Rey, M.V., Yamaji, S., Saffrey, P., Margoninski, O., Bogle, I., Finkelstein, A., *et al.*: A composite computational model of liver glucose homeostasis. i. building the composite model. Journal of The Royal Society Interface **9**(69), 689–700 (2011)
27. Wallace, S.W.: Decision making under uncertainty: Is sensitivity analysis of any use? Operations Research
48(1), 20–25 (2000)
28. Cooling, M.: Modelling the inositol 1, 4, 5-trisphosphate/calcineurin signal transduction pathway in the cardiac myocyte. PhD thesis, ResearchSpace@ Auckland (2007)
29. Bandara, S., Schlöder, J.P., Eils, R., Bock, H.G., Meyer, T.: Optimal experimental design for parameter estimation of a cell signaling model. PLoS computational biology **5**(11) (2009)
30. Gutenkunst, R.N., Waterfall, J.J., Casey, F.P., Brown, K.S., Myers, C.R., Sethna, J.P.: Universally sloppy parameter sensitivities in systems biology models. PLoS computational biology **3**(10), 189 (2007)
31. Moré, J.J.: The levenberg-marquardt algorithm: implementation and theory. In: Numerical Analysis, pp. 105–116. Springer, ??? (1978)
32. Branch, M.A., Coleman, T.F., Li, Y.: A subspace, interior, and conjugate gradient method for large-scale bound-constrained minimization problems. SIAM Journal on Scientific Computing **21**(1), 1–23 (1999)
33. Transtrum, M.K., Sethna, J.P.: Improvements to the levenberg-marquardt algorithm for nonlinear least-squares minimization. arXiv preprint arXiv:1201.5885 (2012)
34. Campolongo, F., Cariboni, J., Saltelli, A.: An effective screening design for sensitivity analysis of large models. Environmental modelling & software **22**(10), 1509–1518 (2007)
35. Saltelli, A., Tarantola, S., Campolongo, F., Ratto, M.: Sensitivity analysis in practice: a guide to assessing scientific models. Chichester, England (2004)
36. Sobol, I.M.: Global sensitivity indices for nonlinear mathematical models and their monte carlo

estimates. Mathematics and computers in simulation **55**(1-3), 271–280 (2001)

37. Saltelli, A.: Making best use of model evaluations to compute sensitivity indices. Computer physics communications **145**(2), 280–297 (2002)
38. Saltelli, A., Annoni, P., Azzini, I., Campolongo, F., Ratto, M., Tarantola, S.: Variance based sensitivity analysis of model output. design and estimator for the total sensitivity index. Computer Physics Communications **181**(2), 259–270 (2010)
39. Refsgaard, J.C., van der Sluijs, J.P., Højberg, A.L., Vanrolleghem, P.A.: Uncertainty in the environmental modelling process–a framework and guidance. Environmental modelling & software **22**(11), 1543–1556 (2007)
40. Saltelli, A., Tarantola, S., Campolongo, F., *et al.*: Sensitivity anaysis as an ingredient of modeling. Statistical Science **15**(4), 377–395 (2000)
41. Pappenberger, F., Iorgulescu, I., Beven, K.J.: Sensitivity analysis based on regional splits and regression trees (sars-rt). Environmental Modelling & Software **21**(7), 976–990 (2006)
42. Helton, J.C., Davis, F.J.: Latin hypercube sampling and the propagation of uncertainty in analyses of complex systems. Reliability Engineering & System Safety **81**(1), 23–69 (2003)
43. Oakley, J.E., O'Hagan, A.: Probabilistic sensitivity analysis of complex models: a bayesian approach. Journal of the Royal Statistical Society: Series B (Statistical Methodology) **66**(3), 751–769 (2004)
44. Ratto, M., Tarantola, S., Saltelli, A.: Sensitivity analysis in model calibration: Gsa-glue approach. Computer Physics Communications **136**(3), 212–224 (2001)
45. Chan, K., Saltelli, A., Tarantola, S.: Sensitivity analysis of model output: variance-based methods make the difference. In: Winter Simulation Conference, pp. 261–268 (1997)
46. Wofsy, C., Kent, U.M., Mao, S.-Y., Metzger, H., Goldstein, B.: Kinetics of tyrosine phosphorylation when ige dimers bind to fc receptors on rat basophilic leukemia cells. Journal of Biological Chemistry **270**(35), 20264–20272 (1995)
47. Cooling, M.T.: Modelling the inositol 1,4,5-trisphosphate/calcineurin signal transduction pathway in the cardiac myocyte (2007)
48. Pfeiffer, J.R., Oliver, J.M.: Tyrosine kinase-dependent assembly of actin plaques linking fc epsilon r1 cross-linking to increased cell substrate adhesion in rbl-2h3 tumor mast cells. The Journal of Immunology **152**(1), 270–279 (1994)
49. Barker, S.A., Caldwell, K.K., Hall, A., Martinez, A.M., Pfeiffer, J., Oliver, J., Wilson, B.: Wortmannin blocks lipid and protein kinase activities associated with pi 3-kinase and inhibits a

subset of responses induced by fc epsilon r1 cross-linking. Molecular Biology of the Cell **6**(9), 1145–1158 (1995)

50. Hatakeyama, M., Kimura, S., Takashi, N., Kawasaki, T., Yumoto, N., Ichikawa, M., Jae-Hoon, K., Saito, K., Saeki, M., Shirouzu, M., *et al.*: A computational model on the modulation of mitogen-activated protein kinase (mapk) and akt pathways in heregulin-induced erbb signalling. Biochemical Journal **373**(2), 451–463 (2003)

Figures

Figure 1 Schematic representation of TNF*α* and IFN*γ* secretions induced by HLA-G signalling pathway.

Figure 2 A phylogenetic tree showing the evolutionary relationships among existing and new sub-models of the pathway. Sub-models highlighted in green boxes mean experimental data exists.

Figure 3 Pathway of interest from Dupont & Erneux model [17].

Figure 4 Simulation of Ca^{2+} and IP3 obtained in OpenCOR without the production of IP4. The URL link for the SED-ML file is https://models.physiomeproject.org/workspace/4f9/

Figure 5 Pathway of interest from the Cooling et al. model [18]. To illustrate the details of the reaction, we show the translocation reaction in this diagram.

Figure 6 Schematic diagram of the *FCERIγ* signalling pathways

Figure 7 The best fit for phosphorylation of Grb2. Blue curves show model predictions and red points are observed experimental data in Tsang et al. [23].

Figure 8 The best fit for phosphorylation of FC*E* (left) and phosphorylation of Syk (right). Blue curves show model predictions and red points are observed experimental data from Faeder et al. [24]. The SED-ML is available at https://models.physiomeproject.org/workspace/519/file/ee26a7df740670259ed8604d2a79b1010662ddea/FCepsilonRI_module/FCepsilonRI_Faederdata.sedml.

Figure 9 Fitted model to data from Rajagopalan et al. [25].

Table 1 Fitted parameters to experimental data from Tsang et al. [23].

Parameter	Description	Value	Source
k_{f1}	FC-pLyn binding rate	58.3902 $\mu M^{-1}.s^{-1}$	Fitted value
k_{f2}	FC phosphorylation rate	0.00817889 s^{-1}	Fitted value
k_{f3}	Lyn phosphorylation rate	1.0887 $\mu M^{-1}.s^{-1}$	Fitted value
k_{f4}	pFC-Syk binding rate	10.5797 $\mu M^{-1}.s^{-1}$	Fitted value
k_{f5}	Syk phosphorylation rate	63.6727 s^{-1}	Fitted value
k_{f6}	pSyk-Grb2 binding rate	0.414288 $\mu M^{-1}.s^{-1}$	Fitted value
k_{f7}	Grb2 phosphorylation rate	11.4185 s^{-1}	Fitted value
k_{r1}	FC-pLyn dissociation rate	0.013548 s^{-1}	Fitted value
k_{r4}	pFC-Syk dissociation rate	0.0806961 s^{-1}	Fitted value
k_{r6}	pSyk-Grb2 dissociation rate	0.731255 s^{-1}	Fitted value

Table 2 Fixed kinetic parameters in this subsequence fitting.

Parameter	Value	Units
k_{f2}	0.00817889	s^{-1}
k_{f4}	10.5797	$\mu M^{-1}.s^{-1}$
k_{f6}	0.414288	$\mu M^{-1}.s^{-1}$
k_{f7}	11.4185	s^{-1}

Table 3 Kinetic parameters to fit to data in Faeder et al. [24] and the boundaries condition.

Parameter	Lower bound	Upper bound
k_{f1}	$10^{-1.5}$	10^{2}
k_{f3}	10^{-3}	10^{2}
k_{f5}	10^{1}	10^{2}
k_{r1}	10^{-3}	10^{1}
k_{r4}	10^{-3}	$10^{0.5}$
k_{r6}	10^{-3}	10^{0}
Pi	10^{-3}	10^{2}

Table 4 Re-fitted parameters that the previous fitted model was not sensitive to. The model was fitted to data set from Faeder et al. [24]. The previous parameters is shown in Table 8.

Parameter	**Description**	**Value**	**Source**
k_{f1}	FC-pLyn binding rate	54.7678 μM^{-1}.s^{-1}	Fitted value
k_{f3}	Lyn phosphorylation rate	0.0035 μM^{-1}.s^{-1}	Fitted value
k_{f5}	Syk phosphorylation rate	33.7157 s^{-1}	Fitted value
k_{r1}	FC-pLyn dissociation rate	0.0031 s^{-1}	Fitted value
k_{r4}	pFC-Syk dissociation rate	0.1174 s^{-1}	Fitted value
k_{r6}	pSyk-Grb2 dissociation	0.481 s^{-1}	Fitted value

Table 5 The parameters for FC*E*RIγ model fitted to data set from Tsang et al. [23] and Faeder et al.[24]. The fourth column listed parameters that can be fitted or fixed in calibration of subsequent components due to the sensitivity analysis.

Parameter	**Value**	**Source**	Status
k_{f1}	54.7678 μM^{-1}.s^{-1}	Fitted to [24]	Fit
k_{f2}	0.00817889 s^{-1}	Fitted to [23]	Fix
k_{f3}	0.0035 μM^{-1}.s^{-1}	Fitted to [24]	Fix
k_{f4}	10.5797 μM^{-1}.s^{-1}	Fitted to [23]	Fit
k_{f5}	33.7157 s^{-1}	Fitted to [24]	Fit
k_{f6}	0.414288 μM^{-1}.s^{-1}	Fitted to [23]	Fit
k_{f7}	11.4185 s^{-1}	Fitted to [23]	Fix
k_{r1}	0.0031 s^{-1}	Fitted to [24]	Fit
k_{r4}	0.1174 s^{-1}	Fitted to [24]	Fit
k_{r6}	0.481 s^{-1}	Fitted to [24]	Fit

Table 6 Fitted parameters to data from Rajagopalan et al. [25].

Parameter	Description	Value	Source
hGactivating/k_{f10}	KIR2DL4-HLA-G binding rate	0.0141 μM^{-1}.s^{-1}	Fitted value
hGactivating/k_{r10}	KIR2DL4-HLA-G dissociation rate	0.0140 s^{-1}	Fitted value
FCepsilonRI/k_{f1}	pLyn binding rate	6.1804 μM^{-1}.s^{-1}	Fitted value
FCepsilonRI/k_{f5}	Syk phosphorylation rate	0.8040 s^{-1}	Fitted value
FCepsilonRI/kr_1	pLyn dissociation rate	0.0015 s^{-1}	Fitted value
hG_FC/k_{f21}	FC binding rate	0.0165 μM^{-1}.s^{-1}	Fitted value
hG_FC/k_{r21}	FC dissociation rate	0.0517 s^{-1}	Fitted value
PI3K/k_{f2}	pGrb2-PI3K binding rate	8.9165 μM^{-1}.s^{-1}	Fitted value
PI3K/kr_2	pGrb2-PI3K dissociation rate	0.0061 s^{-1}	Fitted value
PI3K/k_{f3}	PI3K activation rate	14.6231 s^{-1}	Fitted value
cytokine/k_{f4}	IFNγ production rate	0.0684 s^{-1}	Fitted value
cytokine/k_{f5}	TNFα production rate	23.1163 s^{-1}	Fitted value
cytokine/k_{f31}	TNFα secretion rate	0.0291 s^{-1}	Fitted value
cytokine/k_{f32}	IFNγ secretion rate	9.7858e-03 s^{-1}	Fitted value
NFAT Cycling equations/k_{f21}	$NFATp_c$ binding rate	0.0516 μM^{-1}.s^{-1}	Fitted value
NFAT Cycling equations/k_{f22}	$NFATN_c$ translocation rate	0.0030 s^{-1}	Fitted value
NFAT Cycling equations/k_{f23}	$NFATN_n$ rephosphorylation rate	0.0022 s^{-1}	Fitted value
NFAT Cycling equations/k_{f24}	$NFATNp_n$ translocation rate	0.9844 s^{-1}	Fitted value
NFAT Cycling equations/k_{r21}	$NFATp_c$ dissociation rate	2.0772 s^{-1}	Fitted value
NFAT Cycling equations/k_{r23}	$NFATp_n$ dephosphorylation rate	0.3345 μM^{-1}.s^{-1}	Fitted value

Table 7 Initial conditions for the FC*E*RIγ signalling sub-model

Parameter	Value	Units	Source
FCE	1	μM	[23]
Syk	0.005	μM	[23]
Grb2	6.47	μM	Estimation
pLyn	6.5	μM	Estimation

Table 8 Initial conditions for the FCεRIγ signalling sub-model

Parameter	Estimation 1	Source	Estimation 2	Units
FCE	0.474	[24]	0.0474	μM
pLyn	0.0332	[24]	0.0474	μM
Syk	0.432	[24]	0.025	μM
Grb2	nil	nil	0.01	μM

Table 9 Parameters to fit to the data in Rajagopalan et al. [25] and the boundaries condition.

Parameter	Lower bound	Upper bound
FCepsilonRIk_{f1}	10^{2}	10^{-3}
FCepsilonRIk_{f5}	10^{1}	10^{2}
FCepsilonRIk_{r1}	10^{-3}	10^{1}
FCepsilonRIk_{r4}	10^{-3}	10^{0}
FCepsilonRIk_{r6}	10^{-3}	10^{0}
cytokines/v 4	10^{-5}	10^{3}
cytokines/v 5	10^{-5}	10^{3}
cytokines/K 4	10^{-5}	10^{3}
cytokines/K 5	10^{-5}	10^{3}
PI3K/k_{f2}	10^{-3}	10^{2}
PI3K/k_{r2}	10^{-3}	10^{2}
PI3K/k_{f3}	10^{-3}	10^{2}
hG FC/k_{f1}	10^{-3}	10^{2}
hG FC/k_{r1}	10^{-3}	10^{2}
hG FC/k_{f1}	10^{-3}	10^{2}
NFAT Cycling/dl4cytokines parameter/k_{f1}	10^{0}	10^{2}
NFAT Cycling/dl4cytokines parameter/k_{f5}	10^{1}	10^{2}
NFAT Cycling/dl4cytokines parameter/k_{r1}	10^{-3}	-10^{0}
NFAT Cycling/dl4cytokines parameter/k_{r4}	10^{-3}	10^{0}
NFAT Cycling/dl4cytokines parameter/k_{r6}	10^{-3}	-10^{0}
NFAT Cycling/dl4cytokines parameter/k_{f10}	10^{-3}	10^{2}
NFAT Cycling/dl4cytokines parameter/k_{r10}	10^{-3}	10^{2}

Table 10 HLA-G cytokines model initial conditions.

Parameter	Value	Units	Source
KIR2DL4	0.098	μM	[25]
PI3K	0.01	μM	[50]
HLA-G	0.1052	μM	[25]
plc	1.3	μM	Estimation

Tables Additional Files

Additional file 1 — The sensitivity of the *FCERIγ* model solutions around the 'best fit' to a selection ofparameters from Tsang et al..
Additional file 2 — The sensitivity of the *FCERIγ* model solutions around the 'best fit' to a selection ofparameters from Faeder et al..
Additional file 3 — The sensitivity of the HLA-G cytokines model solutions around the 'best fit' to a selection ofparameters.
Additional file 4 — Flow chart of steps in re-using and importing components into a new model.
Additional file 5 — Overall structure of the top level CellML model showing the encapsulation hierarchy, the CellMLmodel imports and the other key parts (units, components, and mappings).

Declaration

Ethics approval and consent to participate

Not applicable

Consent for publication

Not applicable

Availability of data and materials

The datasets generate and/or analysed during the current study are available in the GitHub repository,

1. Ca^{2+} oscillations in Dupont and Erneux, 1997
   https://github.com/Nurulizza/HLAG_to_cytokine/tree/master/dupont_1997
2. NFAT cycling in Cooling et al., 2009
   https://github.com/Nurulizza/HLAG_to_cytokine/tree/master/cooling_2009
3. FCεRIγ submodel

https://github.com/Nurulizza/HLAG_to_cytokine/blob/master/FCepsilonRI.cellml

4. HLA-G cytokines model
   https://github.com/Nurulizza/HLAG_to_cytokine

Competing interests

The authors declare that they have no competing interests

Funding

Not applicable

Authors' contributions

NII collected and interpreted the data from literature. NII generated and run the simuations. NII conceived and design the analysis, and was a single contributor in writing the manuscript.

Acknowledgements

This paper and the research behind it would not have been possible without the patient guidance, exceptional support and useful critiques of my supervisors, Associate Professor Alys R Clark and Dr David Nickerson at Auckland Bioengineering Institute, The University of Auckland.

Figures

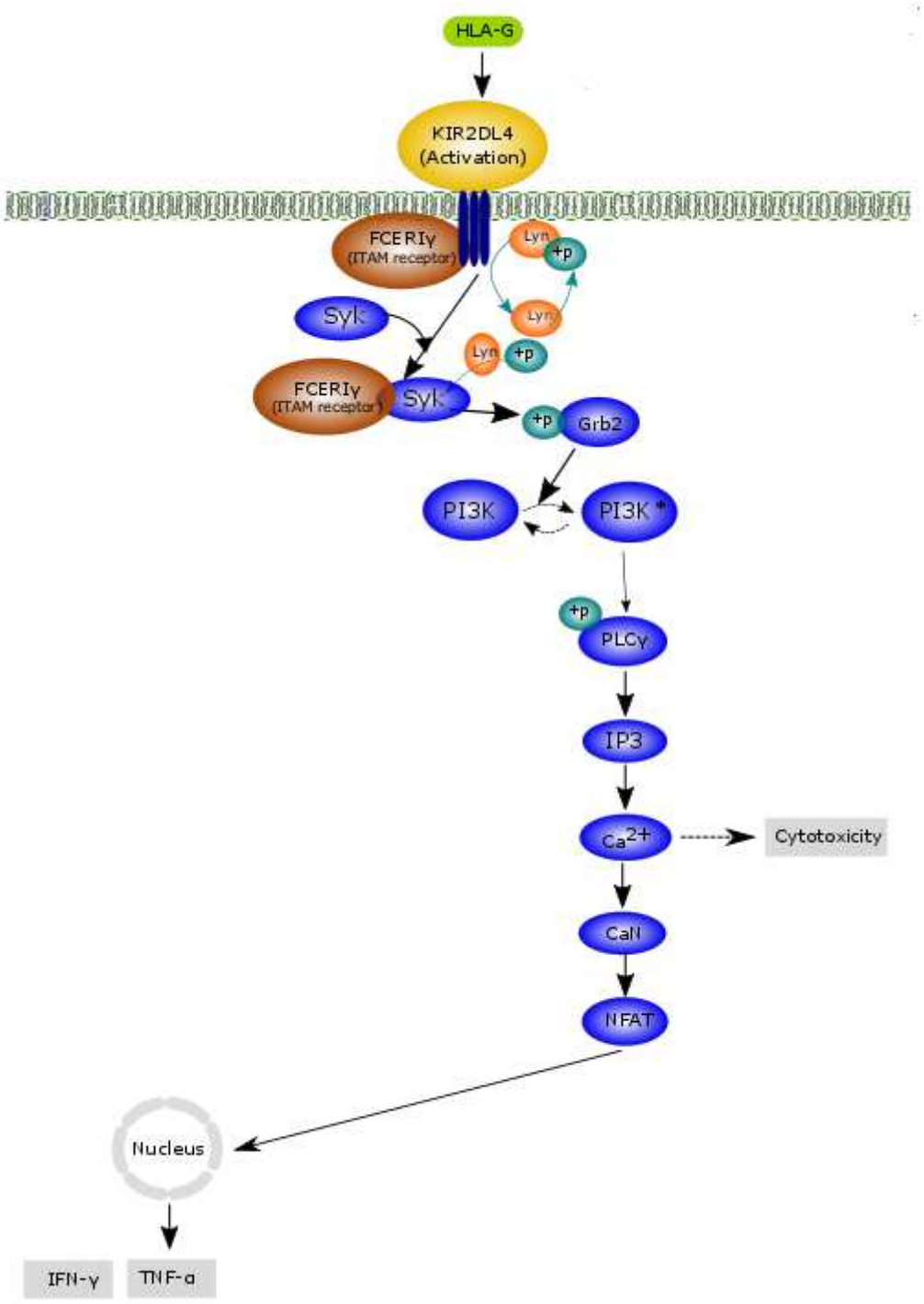

Figure 1

Schematic representation of TNFα and IFNγ secretions induced by HLA-G signalling pathway.

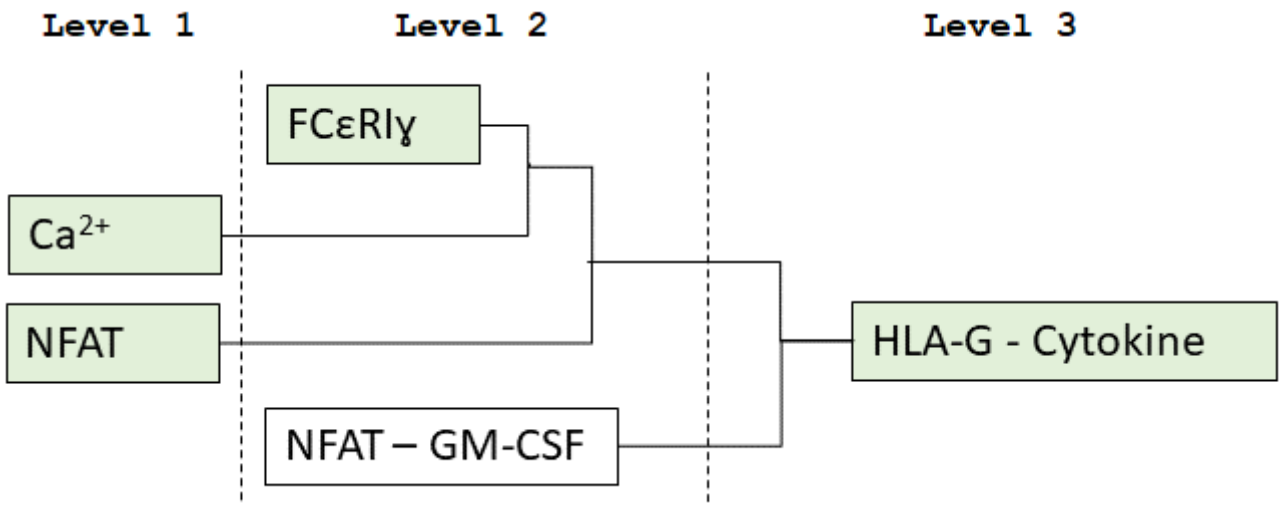

Figure 2

A phylogenetic tree showing the evolutionary relationships among existing and new sub-models of the pathway. Sub-models highlighted in green boxes mean experimental data exists.

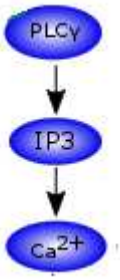

Figure 3

Pathway of interest from Dupont & Erneux model [17].

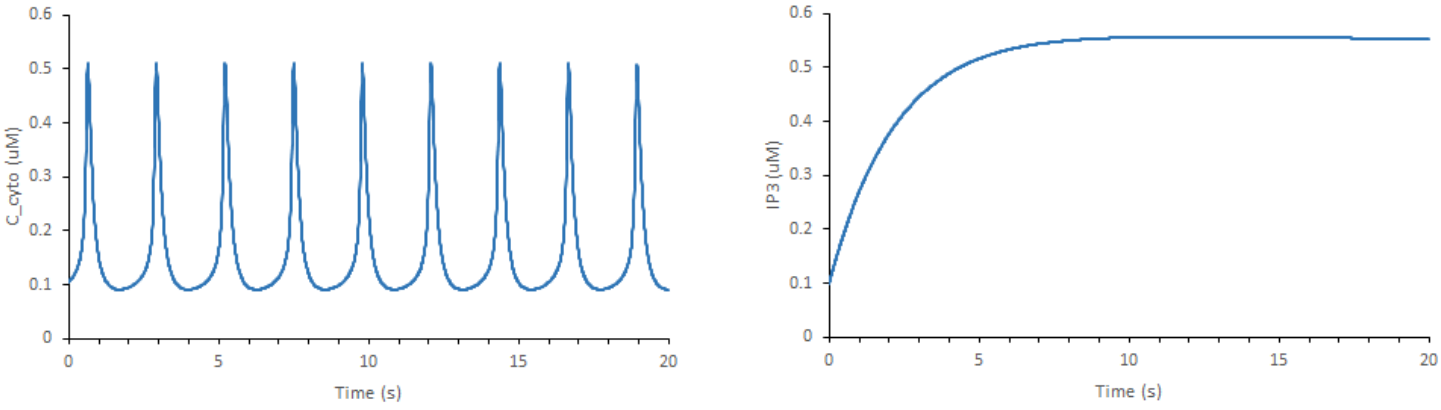

Figure 4

Simulation of Ca2+ and IP3 obtained in OpenCOR without the production of IP4. The URL link for the SED-ML file is https://models.physiomeproject.org/workspace/4f9/

file/a779f6ed1fef6592a6646dfd539413b47e56ac04/test_dupont

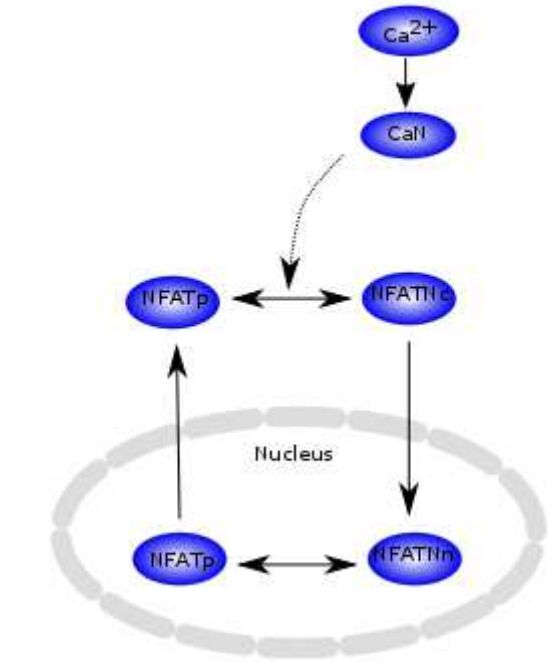

Figure 5

Pathway of interest from the Cooling et al. model [18]. To illustrate the details of the reaction, we show the translocation reaction in this diagram.

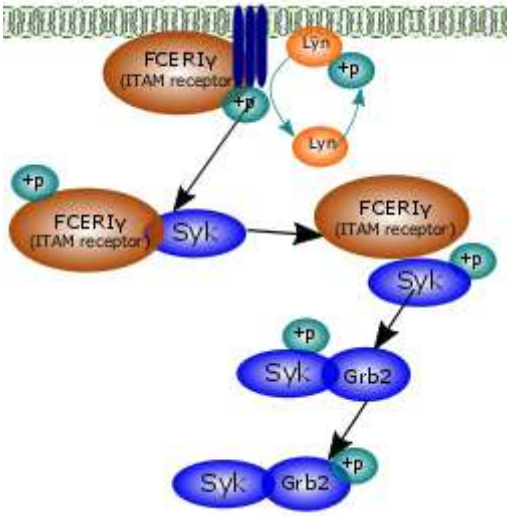

Figure 6

Schematic diagram of the F CERIγ signalling pathways

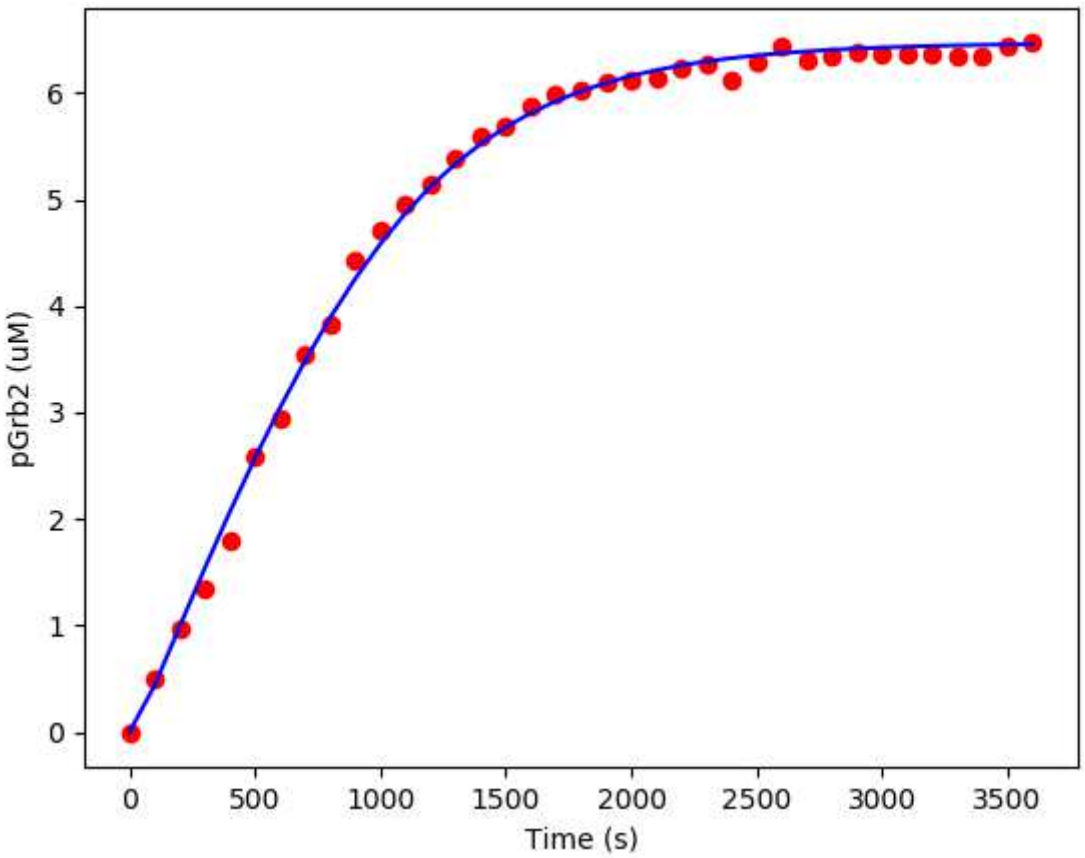

Figure 7

The best fit for phosphorylation of Grb2. Blue curves show model predictions and red points are observed experimental data in Tsang et al. [23].

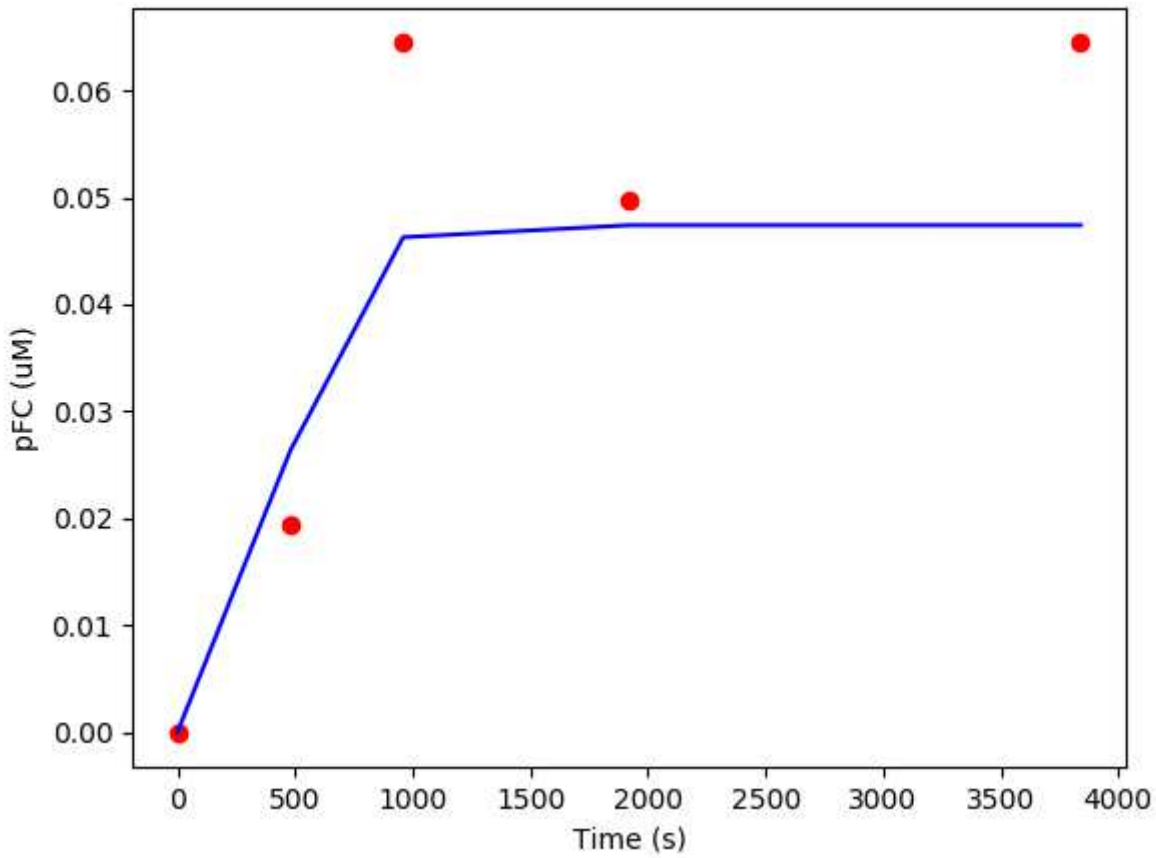

Figure 8

The best fit for phosphorylation of FCE (left) and phosphorylation of Syk (image not available with this version). Blue curves show model predictions and red points are observed experimental data from Faeder et al. [24].

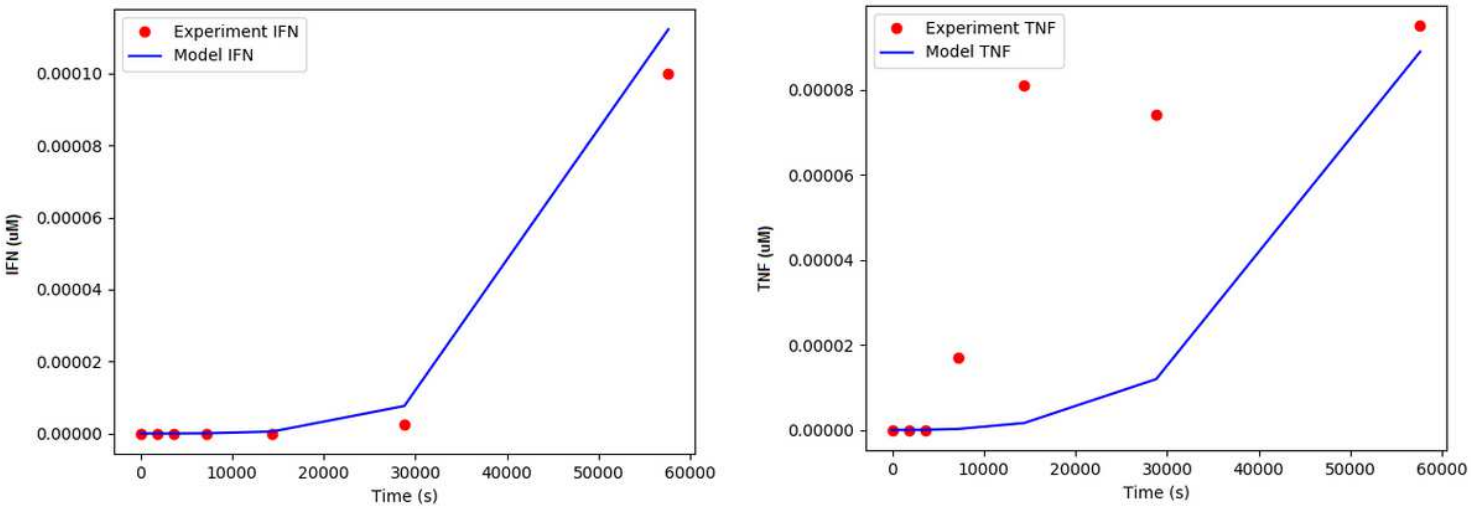

Figure 9

Fitted model to data from Rajagopalan et al. [25].

Supplementary Files

This is a list of supplementary files associated with this preprint. Click to download.

- AdditionalFile1.pdf
- AdditionalFile2.pdf
- AdditionalFile3.pdf
- AdditionalFile4.pdf
- AdditionalFile5.pdf